JUNE 18 2026

A digital-filter model for simulating sound absorption in the air

Rubén Fraile ; Juan José Gómez-Alfageme ; Elena Blanco-Martín ; Juana María Gutiérrez-Arriola ; Nicolás Sáenz-Lechón

J. Acoust. Soc. Am. 159, 5554–5565 (2026)
https://doi.org/10.1121/10.0044114

JASA ARTICLE

A digital-filter model for simulating sound absorption in the air

Rubén Fraile,[a] Juan José Gómez-Alfageme, Elena Blanco-Martín, Juana María Gutiérrez-Arriola, and Nicolás Sáenz-Lechón
CEIMM, Universidad Politécnica de Madrid, Campus Sur, Madrid 28031, Spain

ABSTRACT:
Absorption in air is often overlooked in acoustic propagation simulations, largely due to the lack of low-complexity, valid, and robust modelling techniques. This paper proposes modelling air absorption using a third-order digital filter whose coefficients are derived analytically from the propagation conditions (temperature, pressure, relative humidity, and propagation distance) and the sampling frequency. The proposed filters closely approximate the absorption model specified in the ISO 9613 standard [(1997). 9613-1, International Standards Organization, Geneva, Switzerland]. Errors remain below 50% for 95% of the frequency spectrum between 20 Hz and 20 kHz for propagation distances of up to 25 m, across atmospheric conditions spanning temperatures from −20 °C to 50 °C, relative humidity from 0% to 100%, and pressures from 97 300 Pa to 104 700 Pa. Although accuracy decreases with increasing distance, similar levels are preserved for propagation distances of up to 100 m when the temperature is below 20 °C. The filters are minimum-phase, enabling not only low-cost simulation of air absorption but also stable inverse filtering to remove air-absorption effects from measured acoustic impulse responses. https://doi.org/10.1121/10.0044114

(Received 13 November 2025; revised 4 May 2026; accepted 21 May 2026; published online 18 June 2026)

[Editor: James F. Lynch] Pages: 5554–5565

I. INTRODUCTION

Absorption of acoustic energy in waves transmitted through air is mainly the result of two physical phenomena (Evans *et al.*, 1972): conversion of mechanical energy of moving molecules into heat (classical losses) and relaxation losses related to the conversion of translational energy into internal molecular energy. Among all of the components of air, only the molecules of the two most abundant (N_2 and O_2) play a relevant role in this second phenomenon (Bass *et al.*, 1990). The magnitude of sound absorption losses is frequency dependent and mainly depends on propagation distance and three atmospheric variables (Bass *et al.*, 1990): atmospheric pressure, temperature, and humidity.

According to the standard mathematical model for sound absorption proposed by the standard ISO 9613-1:1993 (ISO, 1993), the absorption losses in decibels are a linear function of the propagation distance,

$$20 \log_{10}\left(\frac{p_l}{p_s}\right) = -\alpha d, \tag{1}$$

where p_s is the amplitude of the pressure wave generated by the source, p_l is the hypothetical amplitude of the pressure wave at the listener position if absorption in air were the only cause of loss, and d is the distance (given in m) between source and listener.

The factor α can be modelled as the addition of three terms dependent on acoustic frequency f,

$$\alpha = \alpha_1 f^2 + \alpha_2 \frac{f_{rN} f^2}{f^2 + f_{rN}^2} + \alpha_3 \frac{f_{rO} f^2}{f^2 + f_{rO}^2}, \tag{2}$$

where

$$\alpha_1 = 1.598\,20 \times 10^{-10} \frac{p_{ref}}{p_0}\sqrt{\frac{T}{T_{ref}}}, \tag{3}$$

$$\alpha_2 = 0.927\,653 \sqrt{\frac{T_{ref}^5}{T^5}} e^{-3352/T}, \tag{4}$$

$$\alpha_3 = 0.110\,745 \sqrt{\frac{T_{ref}^5}{T^5}} e^{-2239.1/T}, \tag{5}$$

where p_0 is the air pressure in Pa, $p_{ref} = 101\,325$ Pa is the reference air pressure, T is temperature in K, $T_{ref} = 293.15$ K is the reference temperature, and f_{rN} and f_{rO} are the relaxation frequencies of nitrogen and oxygen, respectively.

Although α_1 depends on pressure and temperature, and α_2 and α_3 only depend on temperature, f_{rN} and f_{rO} also depend on humidity, according to

$$f_{rN} = \frac{p_0}{p_{ref}}\sqrt{\frac{T_{ref}}{T}}\left(9 + 280h \times e^{4.17\left(1-\sqrt[3]{T_{ref}/T}\right)}\right), \tag{6}$$

$$f_{rO} = \frac{p_0}{p_{ref}}\left(24 + 4.04 \times 10^4 h \frac{0.02 + h}{0.391 + h}\right), \tag{7}$$

where h is the molar concentration of water vapour in %. This can be estimated from the relative humidity H, which is also given in % as (Attenborough *et al.*, 2007, Chap. 1)

[a]Email: r.fraile@upm.es

https://doi.org/10.1121/10.0044114

$$h = H\left(\frac{p_{\mathrm{sat}}}{p_{\mathrm{ref}}}\right)\left(\frac{p_{\mathrm{ref}}}{p_0}\right), \tag{8}$$

where p_{sat} is the saturated vapour pressure, which can be approximated by

$$\frac{p_{\mathrm{sat}}}{p_{\mathrm{ref}}} \approx 10^{4.6151-6.8346(T_{\mathrm{ref}}/T)^{1.261}}. \tag{9}$$

The complexity of this model makes its direct use in real-time applications challenging. Only in recent years has it been incorporated into real-time systems but implemented on hardware with very high computational power. In particular, Mainolfi (2025) implemented the model in an auralization system running on a platform equipped with a 14-core central processing unit (CPU) and a 30-core graphical processing unit (GPU). Despite these limitations, modelling air absorption in room acoustic simulations is essential to avoid significant errors at frequencies above 1 kHz (Okuzono, 2024). Motivated by this need, several authors have proposed simplified approaches based on digital filters designed to reproduce the frequency-dependent behaviour of air absorption.

Early work by Huopaniemi *et al.* (1997) introduced the use of a first-order infinite impulse response (IIR) filter, with parameters determined by numerically fitting the ISO 9613 absorption model (ISO, 1993). However, the complexity of the frequency response—which may exhibit a frequency-dependent attenuation with variable slope—suggests that a single first-order filter is insufficient in many practical situations. Indeed, Eq. (2) shows that the total absorption loss arises from three distinct physical mechanisms acting as cascaded filters, a behaviour that cannot be accurately captured by a single first-order system.

Moreover, the shape of the absorption response strongly depends on atmospheric conditions. In particular, the relative contribution of the second and third terms in Eq. (2) varies significantly with temperature T, pressure p_0, and relative humidity H. To address this dependency, Petruzzellis and Zanghieri (2013) proposed the use of two first-order IIR filters in selected cases, although no explicit procedure for computing filter coefficients was provided. More recently, Kates and Brandewie (2020) suggested a first-order filter with time-varying coefficients obtained through numerical fitting of the ISO 9613 model. Hamilton (2021b,a) aimed to remove the need for numerical optimization by relying on physically motivated formulations; however, both approaches resulted in filters with substantially higher computational cost than low-order IIR solutions.

Finite impulse response (FIR)-based models have also been proposed (Tsuchiya, 2007). In this case, accurately reproducing the complexity of the air-absorption response requires high-order filters, which are associated with long group delays and increased susceptibility to numerical errors. These numerical issues may become particularly critical when inverse filtering is required because they can lead to unstable systems.

In this paper, we propose a digital filter for simulating air absorption based on a cascade of three first-order IIR filters. This approach maintains a low computational cost, resulting in an overall third-order system while preserving a direct link with the underlying physical mechanisms: each filter corresponds to one term in Eq. (2), namely, classical losses, N_2 relaxation losses, and O_2 relaxation losses. The proposed filters are minimum-phase, enabling not only the efficient simulation of air absorption but also stable inverse filtering to remove air-absorption effects from measured acoustic impulse responses. Finally, we derive closed-form analytical expressions that allow all filter parameters to be computed directly from the atmospheric variables T, p_0, and H.

II. FILTER MODEL

As explained in Sec. I, the ISO 9613 model decomposes the attenuation factor $\alpha(\mathrm{dB/m})$ caused by sound absorption in air as the sum of three frequency-dependent terms [Eq. (2)]. As α is defined as the logarithm of the ratio between pressure amplitudes [Eq. (1)], this model is equivalent to defining that ratio as a product of three frequency-dependent factors such that

$$\left|\frac{p_l(f)}{p_s(f)}\right| = |H_1(f)|\cdot|H_2(f)|\cdot|H_3(f)|, \tag{10}$$

where the modulus operator $|\cdot|$ is used because the model does not provide any information about phase.

Our challenge is to find three first-order IIR digital filters, in which response in z-domain is equal to

$$\mathcal{H}_i(z) = k_i \cdot \frac{1-c_i z^{-1}}{1-p_i z^{-1}}, \tag{11}$$

where $i \in \{1,2,3\}$ and $c_i, p_i \in \mathbb{R}$ such that each one is as similar as possible to its corresponding continuous-time model $H_i(f)$ when applying the impulse invariance transformation (Oppenheim *et al.*, 1999, Chap. 7),

$$|\mathcal{H}_i(e^{j2\pi f/f_s})| \sim |H_i(f)|, \tag{12}$$

where f_s is the sampling rate and j is the imaginary unit. We also require that each $\mathcal{H}_i(z)$ is stable to avoid implementation issues and, as the ISO 9613 model provides no information about phase, we further impose the constraint that each $\mathcal{H}_i(z)$ has an inverse system that is also stable. These two conditions imply that

$$|c_i| < 1, \quad |p_i| < 1 \quad \forall i \in \{1,2,3\}. \tag{13}$$

The response of the whole system will be given in z-domain by

$$\mathcal{H}(z) = k_1k_2k_3 \cdot \frac{1-c_1z^{-1}}{1-p_1z^{-1}}\frac{1-c_2z^{-1}}{1-p_2z^{-1}}\frac{1-c_3z^{-1}}{1-p_3z^{-1}}. \tag{14}$$

For simplicity, we will group the multiplicative factors k_i in a single group $k = k_1 k_2 k_3$. Therefore, the challenge is to find the values for the seven parameters k, c_1, c_2, c_3, p_1, p_2, and p_3 that provide the best fit between the digital and ISO 9613 models.

Given $\mathcal{H}(z)$, the frequency response of the digital model in decibels can be written as

$$20 \log_{10}\left|\mathcal{H}_i\left(e^{j2\pi f/f_s}\right)\right| = 20 \log_{10} k + \sum_{i=1}^{3} 20 \log_{10}\left|\frac{1 - c_i e^{-j2\pi f/f_s}}{1 - p_i e^{-j2\pi f/f_s}}\right|. \quad (15)$$

Calculating the moduli

$$20 \log_{10}\left|\mathcal{H}_i\left(e^{j2\pi f/f_s}\right)\right| = 20 \log_{10} k + \sum_{i=1}^{3} 10 \log_{10} \times \left(\frac{1 - 2c_i \cos\left(2\pi \frac{f}{f_s}\right) + c_i^2}{1 - 2p_i \cos\left(2\pi \frac{f}{f_s}\right) + p_i^2}\right). \quad (16)$$

The procedure and criteria for fitting this model to that of Eq. (2) is described in Secs. II A–II C.

A. Model for classical losses

Classical absorption losses are modelled by the first term ($i = 1$) in Eq. (2). Therefore, for this term, Eq. (12) becomes

$$10 \log_{10}\left(\frac{1 - 2c_1 \cos\left(2\pi \frac{f}{f_s}\right) + c_1^2}{1 - 2p_1 \cos\left(2\pi \frac{f}{f_s}\right) + p_1^2}\right) \sim -\alpha_1 d f^2. \quad (17)$$

As shown in Fig. 1(a), the ISO 9613 model for classical losses has a low-pass frequency response that is much simpler than that of the full model. We, therefore, propose a simple one-pole model ($c_1 = 0$). As a criterion for similarity between the ISO 9613 and the digital model, we propose that the 10 dB/km attenuation frequency is the same for both systems. This frequency is

$$-\alpha_1 f_{-10}^2 = -\frac{10}{1000} \rightarrow f_{-10} = \sqrt{\frac{0.01}{\alpha_1}}, \quad (18)$$

and the resulting condition for $\mathcal{H}_i\left(e^{j2\pi f/f_s}\right)$ is

$$20 \log_{10}\left|\frac{\mathcal{H}_i\left(e^{j2\pi 0/f_s}\right)}{\mathcal{H}_i\left(e^{j2\pi f_{-10}/f_s}\right)}\right| = 0.01d. \quad (19)$$

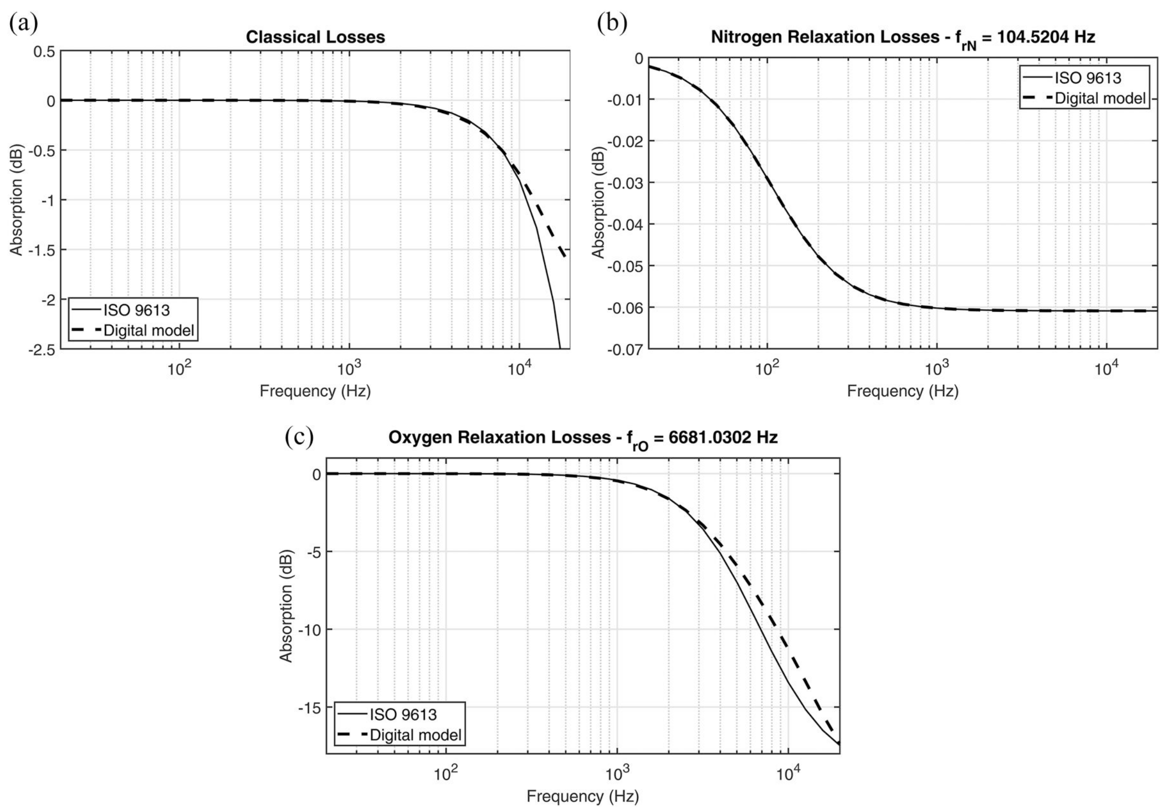

FIG. 1. The three components of absorption losses in air as a function of frequency for $d = 50$ m, $T = 298.15$ K, $p_0 = 101325$ Pa, and $H = 40\%$. Classical losses (a) and relaxation losses associated with N_2 (b) and O_2 (c) molecules are displayed. For the digital model, $f_s = 48$ kHz.

https://doi.org/10.1121/10.0044114

The values of p_1 that satisfy this condition are (see Appendix A)

$$p_1 = \frac{\cos\left(\frac{2\pi}{f_s}\sqrt{\frac{0.01}{\alpha_1}}\right) - 10^{0.001d}}{1 - 10^{0.001d}} \pm \sqrt{\left(\frac{\cos\left(\frac{2\pi}{f_s}\sqrt{\frac{0.01}{\alpha_1}}\right) - 10^{0.001d}}{1 - 10^{0.001d}}\right)^2 - 1}, \quad (20)$$

and the option satisfying $|p_1| < 1$ should be chosen for the system to be stable. Figure 1(a) illustrates the fit between this model and the ISO 9613 model for a distance of 50 m and atmospheric variables $T = 298.15$ K and $p_0 = 101325$ Pa.

B. Model for relaxation losses

According to Eq. (2), relaxation losses for N_2 and O_2 have the same form. Therefore, the modelling problem can be formulated as the search of (c_i, p_i) pairs such that

$$10 \log_{10}\left(\frac{1 - 2c_i \cos\left(2\pi \frac{f}{f_s}\right) + c_i^2}{1 - 2p_i \cos\left(2\pi \frac{f}{f_s}\right) + p_i^2}\right) \sim -\alpha_i d f_{ri} \frac{f^2}{f^2 + f_{ri}^2}, \quad (21)$$

where $i \in \{2, 3\}$, $f_{r2} = f_{r\mathrm{N}}$, and $f_{r3} = f_{r\mathrm{O}}$. Figures 1(b) and 1(c) show the shape of these absorption loss functions $-\alpha_i d f_{ri} f^2/(f^2 + f_{ri}^2)$. It can be noticed that their low-pass behaviour is somewhat more complex than that associated with classical losses because the response has a "backwards-*S*" shape with two corner frequencies. This shape suggests the need for using zero-pole models instead of simpler one-pole models as employed for classical losses.

Considering the shape of the frequency dependence of relaxation losses, we propose the following requirements for the design of the digital model corresponding to each component:

(I) The system must be low pass;

(II) attenuation at high frequencies ($f = f_s/2$) with respect to $f = 0$ Hz should be as specified by the ISO 9613 model such that

$$L_{f_s/2} = \alpha_i d f_{ri} \frac{\left(\frac{f_s}{2}\right)^2}{\left(\frac{f_s}{2}\right)^2 + f_{ri}^2}; \quad (22)$$

(III) and we further require the system to be minimum-phase so that it has an inverse system that is stable.

1. Nitrogen relaxation losses

Typical relaxation frequencies of nitrogen in air are below 1 kHz (see results in Sec. III). This implies that the frequency response in Eq. (22) reaches its asymptotic behaviour within the audible frequency range [Fig. 1(b)]. Requirements (I) and (II) above refer to this asymptotic behaviour. For nitrogen relaxation, we propose to design a zero-pole model that complies with the next additional requirement:

(IV) Attenuation at the relaxation frequency $f_{r2} = f_{r\mathrm{N}}$ should be equal to the ISO 9613 model such that

$$\alpha_2 d f_{r\mathrm{N}} \frac{f^2}{f^2 + f_{r\mathrm{N}}^2}\bigg|_{f=f_{r\mathrm{N}}} = \frac{1}{2}\alpha_2 d f_{r\mathrm{N}}. \quad (23)$$

Taking into account all four requirements, the pair (c_2, p_2) can be obtained as follows (see Appendix B for a detailed derivation):

(1) Calculate

$$\Lambda_{2,f_s/2} = 10^{L_{f_s/2}/20}, \quad (24)$$

$$\Lambda_{2,f_{r\mathrm{N}}} = 10^{\alpha_2 d f_{r\mathrm{N}}/10}, \quad (25)$$

$$\xi_2 = \cos(2\pi f_{r\mathrm{N}}/f_s), \quad (26)$$

where f_s is the sampling rate of the digital system;

(2) use the previous values to calculate

$$\chi_2 = \frac{\left(\Lambda_{2,f_{r\mathrm{N}}}^2 - 1\right) - \xi_2\left(1 - \Lambda_{2,f_{r\mathrm{N}}}\right)^2}{\left(1 - \Lambda_{2,f_{r\mathrm{N}}}\right)^2 - \xi_2\left(\Lambda_{2,f_{r\mathrm{N}}}^2 - 1\right)}; \quad (27)$$

(3) from χ_2, calculate the zero of the system as

$$c_2 = -\chi_2 \pm \sqrt{\chi_2^2 - 1}, \quad (28)$$

choosing the solution yielding $|c_2| < 1$; and

(4) after c_2 is known, calculate the pole as

$$p_2 = \frac{\left(1 - \Lambda_{2,f_s/2}\right) + c_2\left(-1 - \Lambda_{2,f_s/2}\right)}{\left(-1 - \Lambda_{2,f_s/2}\right) + c_2\left(1 - \Lambda_{2,f_s/2}\right)}. \quad (29)$$

Figure 1(b) illustrates the fitting between this digital model and the corresponding term in the ISO 9613 model for one specific case.

2. Oxygen relaxation losses

Typical relaxation frequencies of oxygen in air are significantly higher than those of nitrogen, and they may even have values beyond the audible band (see results in Sec. III). Therefore, the asymptotic behaviour of the corresponding losses is often not reached below $f_s/2$ [Fig. 1(c)]. Consequently, requirement (II) only corresponds sometimes to the high frequency asymptotic behaviour of oxygen relaxation losses. In addition, it may even happen that $f_{r\mathrm{O}} > f_s/2$ such that requirement (IV) stated for nitrogen relaxation losses cannot be applied to oxygen relaxation losses. Instead, we proposed the following alternative:

(IV) If $f_{rO} \le 30$ kHz then the attenuation at $f = f_{rO}/3$ should be equal to the ISO 9613 model. We call this reference frequency f_3 and its corresponding losses L_3,

$$L_3 = \alpha_3 d f_{rO} \frac{\frac{f_{rO}^2}{9}}{\frac{f_{rO}^2}{9} + f_{rO}^2} = \frac{1}{10}\alpha_3 d f_{rO}. \quad (30)$$

For higher oxygen relaxation frequencies, the reference frequency remains fixed ($f_3 = 10$ kHz), and its corresponding losses L_3 are

$$L_3 = \alpha_3 d f_{rO} \frac{10^8}{10^8 + f_{rO}^2}. \quad (31)$$

Now, the pair (c_3, p_3) can be obtained as follows (again, see Appendix B for a detailed derivation):

(1) Calculate

$$\Lambda_{3,f_s/2} = 10^{L_{f_s/2}/20}, \quad (32)$$

$$\Lambda_3 = 10^{L_3/10}, \quad (33)$$

$$\xi_3 = \cos(2\pi f_3/f_s); \quad (34)$$

(2) from the previous values,

$$\chi_3 = \frac{\left(\Lambda_3^2 - 1\right) - \xi_3(1-\Lambda_3)^2}{(1-\Lambda_3)^2 - \xi_3\left(\Lambda_3^2 - 1\right)}; \quad (35)$$

(3) then, the zero of the system is

$$c_3 = -\chi_3 \pm \sqrt{\chi_3^2 - 1}, \quad (36)$$

choosing the solution yielding $|c_3| < 1$; and

(4) after c_3,

$$p_3 = \frac{\left(1 - \Lambda_{3,f_s/2}\right) + c_3\left(-1 - \Lambda_{3,f_s/2}\right)}{\left(-1 - \Lambda_{3,f_s/2}\right) + c_3\left(1 - \Lambda_{3,f_s/2}\right)}. \quad (37)$$

Figure 1(c) illustrates the fitting between this digital model and the corresponding term in the ISO 9613 model.

C. Adjustment of the multiplicative factor *k*

The frequency response of the digital model is specified in Eq. (15). For that model, the value of c_1 was set to zero, the value of p_1 can be calculated from Eq. (20), the values of c_2 and c_3 can be calculated using, respectively, Eqs. (28) and (36), and the values of p_2 and p_3 can be derived from Eqs. (29) and (37), respectively. After these are known, the value of k can be obtained by imposing the condition that the response for $f = 0$ equals 0 dB, which is the same as for the ISO 9613 model [recall Eq. (2)]

$$20 \log_{10}\left|\mathcal{H}_i\left(e^{j2\pi f/f_s}\right)\right|_{f=0} = 0. \quad (38)$$

Therefore,

$$20 \log_{10} k + \sum_{i=1}^{3} 20 \log_{10}\left|\frac{1-c_i}{1-p_i}\right| = 0. \quad (39)$$

Taking logarithms away and solving for k,

$$k = (1-p_1)\cdot\frac{1-p_2}{1-c_2}\cdot\frac{1-p_3}{1-c_3}. \quad (40)$$

III. MODEL EVALUATION

As reviewed in Sec. I, the ISO 9613 model for absorption losses in sound transmitted through air estimates such losses for any frequency depending on four parameters: temperature, pressure, humidity, and distance. To assess the capability of the proposed digital model to fit ISO 9613 losses, we have evaluated its performance for a set of 1 080 000 different combinations of values for such parameters, corresponding to the following ranges:

- **Temperature *T*:** According to the standard ISO 9613-1:1993 (ISO, 1993), the ISO 9613 model provides the best loss estimates for temperatures ranging from −20 °C to 50 °C. Values in this interval were chosen with a resolution of 2 °C. Thus, 36 different temperatures were simulated;
- **pressure p_0:** Although the ISO 9613 model provides good loss estimates for pressures up to 2 atm = 202 650 Pa (ISO, 1993), only realistic values for atmospheric pressure (taken from Swiss Federal Office for Meteorology and Climatology, 2025) were simulated. Specifically, pressure values from 97 300 Pa to 104 700 Pa with a resolution of 100 Pa were simulated, resulting in 75 possible values;
- **humidity *H*:** Relative humidity values from 5% to 100% were simulated with a resolution of 5%, resulting in 20 different values; and
- **distance *d*:** Source to receiver distances in large auditorium halls can reach several tens of meters (Gade, 2007). Considering this, we have simulated distances from 5 m to 100 m with a resolution of 5 m. This resulted in 20 different values.

Therefore, all possible combinations of the abovementioned values yielded a number of $36 \times 75 \times 20 \times 20 = 1\,080\,000$ simulation conditions, as mentioned previously. Each condition was simulated for three different sampling frequencies f_s: 44.1, 48, and 96 kHz, thus, yielding 3 240 000 simulations.

A. Validity of assumptions: Relaxation frequencies and molar concentration of water vapour

The limits for the validity of the ISO 9613 model are identified by the standard itself (ISO, 1993). Specifically, these are stated in terms of the relative accuracy of the model for pure-tone signals. The simulated values for

https://doi.org/10.1121/10.0044114

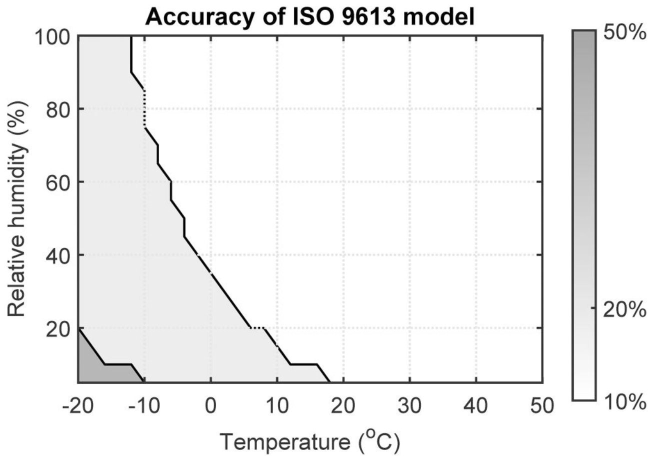

FIG. 2. Worst-case accuracy of the ISO 9613 model as a function of temperature and relative humidity. White area corresponds to 10% relative accuracy, light gray corresponds to 20%, and dark gray corresponds to 50%.

temperature and pressure are within the ranges yielding the best accuracy of the model: 10%. Apart from frequency, the remaining variable affecting accuracy is the molar concentration of water vapour h. This depends on temperature, pressure, and humidity as specified in Eq. (8), although the dependence on pressure is weaker than the others at usual atmospheric conditions.

Figure 2 shows the worst-case accuracy of the ISO 9613 model for all of the simulated pairs of values for temperature and relative humidity (T and H, respectively). The white area (10% relative accuracy) corresponds to pairs for which $0.05\% < h < 5\%$ for all simulated atmospheric pressures. The light gray area (20% relative accuracy) corresponds to combinations for which $0.005\% < h$ for all pressures but $h < 0.05\%$ for some of them. The dark gray area (50% relative accuracy) corresponds to (T, H) pairs for which $h < 0.005\%$ at least for one simulated value of p_0. The plot in Fig. 2 depicts that the relative accuracy of the ISO 9613 model is better than 20% for almost all cases and better than 10% for the majority of cases. We will use these reference accuracies (10%, 20%, and 50%) to evaluate the fitting between our proposed digital model and the ISO 9613 model.

The development of our filter model was partially based on the assumptions that $f_{rN} \ll f_s/2$, and that this condition was not true for f_{rO} (Sec. II B). Figure 3 shows the empirical distributions of the values obtained during simulations for f_{rN} and f_{rO}. As for f_{rN}, all values are below 2 kHz, hence, the condition $f_{rN} \ll f_s/2$ always holds. In contrast, the range of variation for f_{rO} is much larger, reaching values above 22.5 kHz in 20% of cases. This implies, on the one hand, that it cannot be generally assumed that $f_{rN} \ll f_s/2$ and, on the other hand, that the third term in Eq. (2) has a range of variation much larger than the second term. These two reasons justify the different modelling approaches for both terms described in Sec. II B.

B. Overall model evaluation

For each 1 of the 3 240 000 simulations mentioned previously, the frequency-dependent air-absorption losses were calculated according to the ISO 9613 model and the digital-filter model introduced herein. These were calculated for 61 frequency values f_k, uniformly distributed in logarithmic scale between 20 Hz and 20 kHz according to the next rule

$$f_k = 20 \times 10^{1+0.05k}, \qquad \text{where } k = 0, \ldots, 60. \tag{41}$$

For each frequency, we define the error as the deviation in decibels of the digital-filter model with respect to the ISO 9613 model such that

$$e_k = -\alpha(f_k)d - 20 \log_{10}\left|\mathcal{H}\left(e^{j2\pi f_k/f_s}\right)\right|, \tag{42}$$

where $\alpha(f_k)$ are the absorption losses corresponding to frequency f_k in dB/m, as given by Eq. (2); d is the propagation distance in m; and $\mathcal{H}(\cdot)$ is the digital-filter model, as given in Eq. (14).

The empirical distributions of all e_k are summarised in Fig. 4(a). According to the simulation procedure described previously, 3 240 000 experimental values have been obtained for each e_k and their distributions are summarised in the plot using their 5th, 10th, 25th, 50th, 75th, 90th, and 95th percentiles. The graph in Fig. 4(a) shows that the model tends to overestimate the absorption losses for high

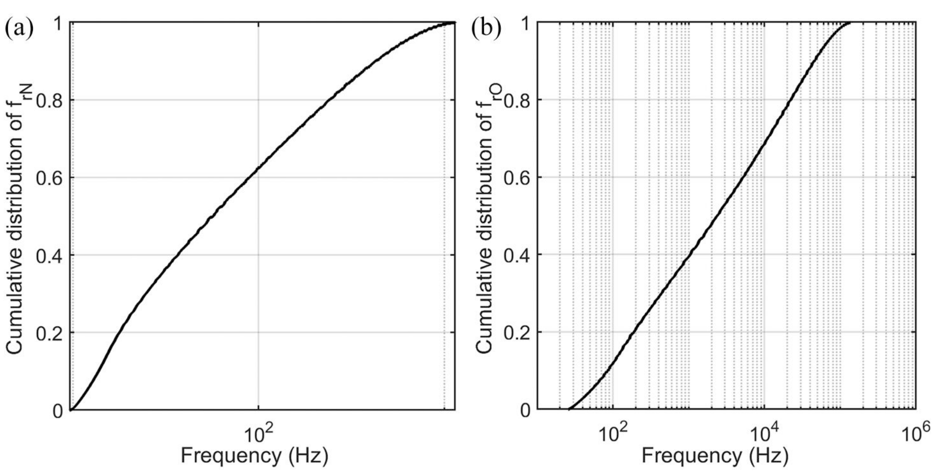

FIG. 3. Cumulative distribution functions of the simulated values for f_{rN} (a) and f_{rO} (b).

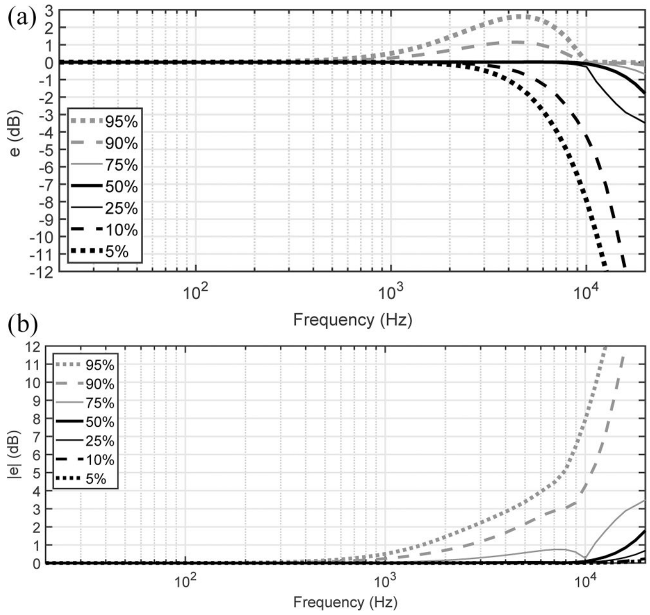

FIG. 4. Distributions of model errors e_k (a) and absolute model errors $|e_k|$ (b) for all frequencies, summarised by means of their percentiles: 5th, 10th, 25th, 50th, 75th, 90th, and 95th.

frequencies. Specifically, beyond 6 kHz, the distributions become skewed toward negative values, as can be observed by looking at the fifth and tenth percentile lines. The plot also indicates that for all frequencies up to 10 kHz, the 25th, 50th, and 75th percentiles are almost coincident at values near 0 dB. This means that the modelling error is almost 0 dB for at least 50% of simulation conditions. For higher frequencies, the model overestimates absorption losses in most cases. Further information about the magnitude of modelling errors can be obtained by analysing the distributions of their absolute values $|e_k|$. These are summarised in Fig. 4(b). The graph shows that although the absolute error reaches values well over 3 dB at high frequencies (over 5 kHz) for a number of cases, the modelling error is kept below 1 dB for frequencies up to 11 kHz in 75% of simulation conditions.

Whereas the previous analysis focuses on the dependence of modelling error on frequency, we are also interested in assessing model performance depending on the atmospheric variables T, p_0, and H and also on distance d and sampling frequency f_s. For that purpose, we use the root mean square error as an overall indicator of model performance, which takes into account the fit over the whole spectrum,

$$e_{\mathrm{rms}} = \sqrt{\frac{1}{61}\sum_{k=0}^{60} e_k^2}. \tag{43}$$

The empirical distribution of e_{rms} for each simulated temperature is summarised by its quartiles in Table I. The values show that the digital model provides close agreement with the ISO 9613 model for temperatures up to approximately 16 °C. The root mean square error is below 1 dB for almost all simulations in that range. From that value upward, the performance of the model worsens, with the worst performance happening between 30 and 36 °C. However, even in those cases, the value of e_{rms} is below 2 dB for more that 50% of simulated conditions and below 4.2 dB for at least 75% of simulated conditions. The values in Table II indicate that the model's performance is also influenced by relative humidity, although the effect is less pronounced than in the case of temperature. In this case, the median of the distributions for all simulated values of relative humidity are approximately constant, where values are below 0.4 dB in all cases. As in the case of temperature, the highest modelling errors happen for intermediate values of relative humidity (around 65%), but in this case, the 75th percentiles of e_{rms} are always below 2 dB. Last, Table III summarises the dependence of the distribution of e_{rms} on distance. These values show that the performance of the digital model in terms of e_{rms} degrades as distance grows. However, the degradation of the median e_{rms} is very limited, where its value is below 1 dB for all simulated distances. It is the upper tail of the distribution that reaches the highest errors, although it is not limited for very long distances: the 75th percentile of e_{rms} is below 1 dB for distances up to 40 m and below 2 dB for distances up to 60 m. Regarding pressure and sampling frequency, no systematic dependence between the distribution of e_{rms} and these variables was observed, therefore, it can be assumed that the performance of the model is independent from p_0 and f_s.

C. Relative error and range of validity

In Sec. III B, we have described the performance of the herein proposed digital-filter modelling approach based on the distributions of absolute errors in the frequency response, which are measured in dB. This analysis has allowed identifying a dependence between that performance and the variables temperature T, relative humidity H, and distance d. From this observation, we now try to assess for which values of these variables the digital filters can provide

TABLE I. Distributions of root mean square errors e_k, summarised by means of their percentiles 25th, 50th, and 75th, for several temperature intervals.

e_{rms} (dB)	Temperature (°C)									
Percentiles	−20 to −14	−12 to −6	−4–2	4–10	12–16	18–22	24–28	30–36	38–44	46–50
25th	0.097	0.099	0.102	0.105	0.113	0.139	0.192	0.260	0.2846	0.226
50th	0.216	0.221	0.227	0.240	0.298	0.443	0.848	1.503	1.634	1.321
75th	0.355	0.363	0.372	0.402	0.589	1.825	3.492	4.155	3.904	3.324

TABLE II. Distributions of root mean square errors e_k, summarised by means of their percentiles 25th, 50th, and 75th, for several intervals of relative humidity.

e_{rms} (dB)	Relative humidity (%)									
Percentiles	5–10	15–20	25–30	35–40	45–50	55–60	65–70	75–80	85–90	95–100
25th	0.109	0.120	0.128	0.132	0.131	0.130	0.128	0.125	0.122	0.118
50th	0.250	0.293	0.323	0.344	0.358	0.366	0.371	0.375	0.376	0.375
75th	0.420	0.541	0.844	1.338	1.608	1.697	1.706	1.640	1.583	1.501

accuracies with respect to the ISO 9613 model that can be considered to be acceptable or, in other words, in which conditions the digital model can be considered to be valid.

As observed in Sec. III A, the accuracy of the ISO 9613 model itself is defined in terms of its relative error, and the standard sets the values of 10%, 20%, and 50% as relevant thresholds for evaluating model validity. Consistently, we can define the accuracy of a digital-filter model in terms of its relative error ϵ_k for each frequency f_k with respect to the ISO 9613 model such that

$$\epsilon_k = \left| \frac{e_k}{\alpha(f_k)d} \right|. \tag{44}$$

From these values, the overall accuracy of the model can be defined as the highest relative error along the spectrum,

$$\epsilon_{\max} = \max_k \epsilon_k. \tag{45}$$

However, evaluating a frequency response of a model in terms of its worst point might be too rigorous. For that reason, we have also used the 95th percentile of ϵ_k to assess model performance,

$$\epsilon_{95\%} = P_{95}(\epsilon_k). \tag{46}$$

The analysis procedure has been given as follows. The values in Table III show that model performance degrades as distance d grows. We have selected a growing sequence of four values of d to analyse such performance degradation: 25, 50, 75, and 100 m. For each of these values of d, we have independently analysed model performance for each possible combination of values for the pair (T, H), which are the other two variables with the most relevant impact on model performance (see Tables II and I). This analysis has consisted of calculating the digital-filter model for all possible combinations of p_0 and f_s (in all, 225 combinations) for that (T, H) pair. For each of these, the values of $\epsilon_{\max}$ and $\epsilon_{95\%}$ defined previously have been calculated, and the highest among all combinations of p_0 and f_s has been taken as an indicator of model performance for the given value of the pair (T, H). Note that this procedure implies selecting the worst case for describing model performance for each value of the (d, T, H) tuple. Figure 5 shows the results for $\epsilon_{\max}$, plotted as maps with coordinates T and H for each one of the aforementioned values for d. Figure 6 shows the same results for $\epsilon_{95\%}$.

Figure 5 shows that the proposed modelling provides accuracies of better than 50% for all frequencies and for all evaluated combinations of p_0, f_s, T, and H if $d = 25$ m. For the same distance, there is a set of values for the (T, H) pair that yields accuracies better than 10% for the whole spectrum. This set corresponds to temperatures between 10 °C and 20 °C when relative humidity is high, above approximately 60%, temperatures between 20 °C and 30 °C with lower humidities, approximately $50\% > H > 25\%$, and very dry atmospheres for higher temperatures. The values in Tables I–III suggest that if this is true for $d = 25$ m, performance is expected to be better for shorter distances. For increasing values of d, particularly 50, 75, and 100 m, Fig. 5 shows that the model cannot achieve accuracies better that 10% for the whole spectrum, although values better than 50% are still obtained for large sets of temperature-humidity combinations. As distance grows, the best performance of the model slightly moves toward lower temperatures and the model begins to yield larger errors for high temperatures.

Figure 4(b) depicts that the largest model errors occur at high frequencies, mainly above 10 kHz, and errors for those frequencies may reach significantly larger values than for the rest of the spectrum. Then, one could reasonably think that evaluating model performance based on the worst point of the spectrum may be too pessimistic. For that reason, we have defined a more relaxed criterion for evaluating model accuracy based on $\epsilon_{95\%}$ as defined previously. The corresponding results are plotted in Fig. 6. Such plots show that if model accuracy is defined as the maximum relative

TABLE III. Distributions of root mean square errors e_k, summarised by means of their percentiles 25th, 50th, and 75th, for several distance intervals.

e_{rms} (dB)	Distance (m)									
Percentiles	5–10	15–20	25–30	35–40	45–50	55–60	65–70	75–80	85–90	95–100
25th	0.016	0.044	0.103	0.163	0.222	0.282	0.342	0.404	0.467	0.533
50th	0.025	0.071	0.135	0.200	0.266	0.333	0.404	0.477	0.556	0.641
75th	0.047	0.095	0.231	0.655	1.248	1.949	2.336	3.566	4.445	5.394

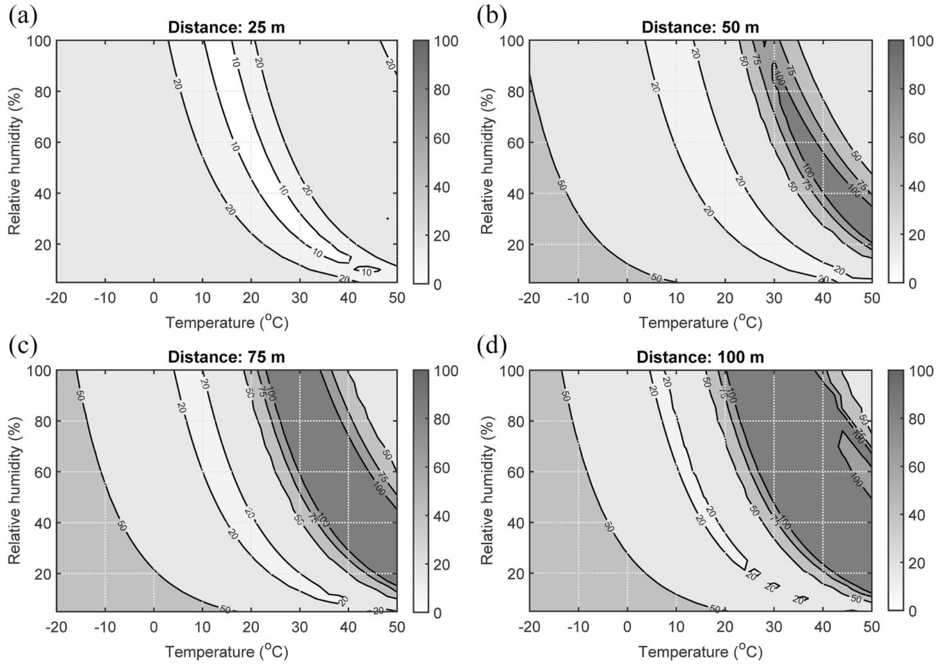

FIG. 5. Model accuracy evaluated as the maximum relative error between the digital-filter and the ISO 9613 models. Each point in the maps corresponds to a (T, H) pair, and its value has been obtained by generating the digital-filter models for that (T, H) pair and all simulated (p_0, f_s) pairs, evaluating the relative error ϵ_{max} for each model, and keeping the greatest ϵ_{max} among all (p_0, f_s) pairs. Each map corresponds to a different distance: 25 m (a), 50 m (b), 75 m (c), and 100 m (d).

error achieved in 95% of the spectrum, then the model achieves accuracies equal to 10% for some combinations of values of temperature and relative humidity for distances up to 100 m, and accuracies better than 50% are achieved for the majority of (T, H) pairs even for $d = 100$ m. A comparative analysis of Figs. 5 and 6 also allows seeing that the conditions for bad model performance are almost the same if this is defined in terms of ϵ_{max} or $\epsilon_{95\%}$. On the (T, H) map, this corresponds approximately to an area with the shape of a curved band that begins around 30 °C for high humidity values and ends around 50 °C for low humidity values. This band gets wider as distance grows and tends to disappear below 50 m.

IV. CONCLUSIONS

In this paper, we have introduced an approach for modelling sound absorption in air using a third-order digital filter. The proposed method takes the ISO 9613 model as a reference and relies on a fully analytic modelling procedure, thereby avoiding computationally expensive optimization processes. The model takes five parameters as inputs: temperature, atmospheric pressure, relative humidity, distance, and the sampling frequency of the digital system. Classical absorption losses are represented first by a one-pole model, whereas nitrogen and oxygen relaxation losses are each modelled using zero-pole structures whose parameters are

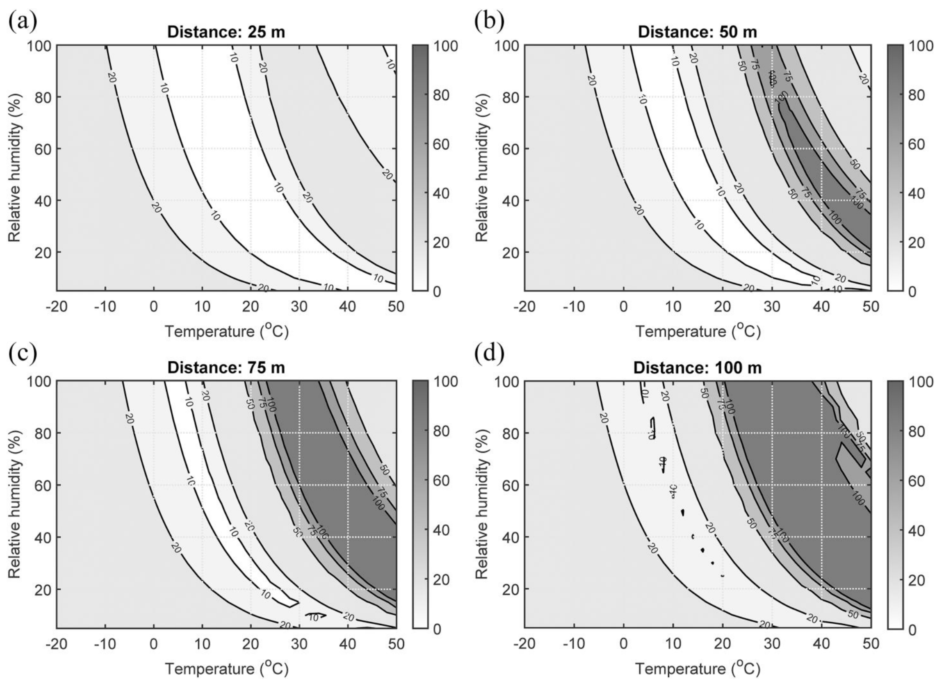

FIG. 6. Model accuracy evaluated as the maximum relative error between the digital-filter and the ISO 9613 models. Each point in the maps corresponds to a (T, H) pair, and its value has been obtained by generating the digital-filter models for that (T, H) pair and all simulated (p_0, f_s) pairs, evaluating the 95th percentile of the relative error $\epsilon_k(\epsilon_{95\%})$ for each model and keeping the greatest $\epsilon_{95\%}$ among all (p_0, f_s) pairs. Each map corresponds to a different distance: 25 m (a), 50 m (b), 75 m (c), and 100 m (d).

analytically derived. A multiplicative gain is then applied to complete the model formulation.

This procedure produces third-order digital filters that are minimum-phase. The low order of the resulting filters has the advantage of allowing simulating sound absorption in air at a low computational cost. Additionally, the fact that the filters are minimum-phase makes it possible to obtain inverse filters that are stable. This makes this modelling approach useful also for removing the effect of sound absorption from measured signals.

The accuracy of the fit between the frequency responses of these digital-filter models and the reference ISO 9613 model has been evaluated for more than 1 000 000 combinations of atmospheric conditions (defined by temperature, pressure, and relative humidity) and distances and for three different sampling frequencies. This accuracy has shown to be independent of pressure and sampling frequency, although fairly dependent on the other three factors, most prominently on distance. Yet, the proposed modelling approach achieves accuracies better than 50% for all analysed frequencies and distances up to 25–40 m, independently of the values of temperature and humidity. For longer distances, the model performance degrades, although accuracies better than 50% for at least 95% of the spectrum are achieved for most temperature-humidity pairs for distances up to 100 m. If improved performance is required under these conditions, it can be achieved by employing higher-order filters.

ACKNOWLEDGMENTS

This research has been performed in the context of project "SonaRe: Patrimonio sonoro del Palacio Real de Madrid. Espacio, acústica y música desde 1746 hasta 1833" (Grant No. PID2023-151325NB-I00), funded by the Spanish government.

AUTHOR DECLARATIONS
Conflict of Interest

The authors have no conflicts to disclose.

DATA AVAILABILITY

Data sharing is not applicable to this article as no new data were created or analysed in this study.

APPENDIX A

Given a one-pole model

$$\mathcal{H}(z) = \frac{1}{1 - pz^{-1}}, \tag{A1}$$

the question approached here is how to calculate p so that the system is low pass and its gain in decibels for a certain frequency f_L equals $-L$ with respect to $f = 0\,\text{Hz}$. This condition can be expressed as

$$20 \log_{10}|\mathcal{H}(e^{j0})| - 20 \log_{10}|\mathcal{H}(e^{j2\pi f_L/f_s})| = L. \tag{A2}$$

As the system is one-pole,

$$20 \log_{10}\left|\frac{1}{1-p}\right| - 20 \log_{10}\left|\frac{1}{1 - pe^{-j2\pi f_L/f_s}}\right| = L. \tag{A3}$$

Calculating both moduli and taking out the logarithms,

$$\frac{1 - 2p\cos\left(2\pi\frac{f_L}{f_s}\right) + p^2}{1 - 2p + p^2} = 10^{L/10}. \tag{A4}$$

This is a second-order equation with standard form

$$p^2 - 2p\frac{\cos\left(2\pi\frac{f_L}{f_s}\right) - 10^{L/10}}{1 - 10^{L/10}} + 1 = 0, \tag{A5}$$

whose solutions are

$$p = \frac{\cos\left(2\pi\frac{f_L}{f_s}\right) - 10^{L/10}}{1 - 10^{L/10}} \pm\sqrt{\left(\frac{\cos\left(2\pi\frac{f_L}{f_s}\right) - 10^{L/10}}{1 - 10^{L/10}}\right)^2 - 1}. \tag{A6}$$

If the system is to be stable, then the solution that satisfies $|p| < 1$ should be chosen.

APPENDIX B

The challenge approached here is finding a first-order discrete-time system with transfer function equal to

$$\mathcal{H}(z) = \frac{1 - cz^{-1}}{1 - pz^{-1}}, \tag{B1}$$

such that its frequency response is as similar as possible to

$$H(f)[\text{dB}] = -L_\infty\frac{f^2}{f^2 + f_r^2}, \tag{B2}$$

where $L_\infty > 0$ is a constant, and f_r is the frequency for which the response equals $-L_\infty/2$. Note that $H(f)$ is a low-pass system such that

$$\begin{aligned} &\max_f H(f) = 0, \quad \arg\max_f H(f) = 0, \\ &\min_f H(f) = -L_\infty, \quad \arg\min_f H(f) = \infty. \end{aligned} \tag{B3}$$

Further, we require that the discrete-time is minimum-phase and stable, which implies $|p| < 1$ and $|c| < 1$, and the system response in time domain is real, which implies that p and c are also real. Similar to Eq. (16), the modulus of the frequency response of $\mathcal{H}(z)$ can be written in decibels for $0 \le f < f_s/2$ as

$$20\log_{10}|\mathcal{H}(e^{j2\pi f/f_s})| = 10\log_{10}\left(\frac{1-2c\cos\left(2\pi\frac{f}{f_s}\right)+c^2}{1-2p\cos\left(2\pi\frac{f}{f_s}\right)+p^2}\right). \quad \text{(B4)}$$

In the search for similarity between both systems, we impose the following constraints to the digital system $\mathcal{H}(z)$:

(1) It should be low pass, as $H(f)$ in Eq. (B3). Therefore,

$$20\log_{10}|\mathcal{H}(f=0)| > 20\log_{10}\left|\mathcal{H}\left(f=\frac{f_s}{2}\right)\right|. \quad \text{(B5)}$$

As the logarithm function is monotonically growing, from Eq. (B4), this constraint results in

$$\frac{1-2c+c^2}{1-2p+p^2} > \frac{1+2c+c^2}{1+2p+p^2} \rightarrow \frac{(1-c)^2}{(1-p)^2} > \frac{(1+c)^2}{(1+p)^2}. \quad \text{(B6)}$$

Because the digital system sought is stable and minimum-phase, $|p|<1$ and $|c|<1$. This implies that $1\pm p$ and $1\pm c$ are always positive. Consequently, the previous expression can be simplified by taking the square root

$$\frac{1-c}{1-p} > \frac{1+c}{1+p}, \quad \text{(B7)}$$

which results in the requirement that $p>c$;

(2) the attenuation at the highest frequency covered by the digital system $(f=f_s/2)$ should be the same for both systems. From Eq. (B3),

$$20\log_{10}|\mathcal{H}(f=0)| - 20\log_{10}\left|\mathcal{H}\left(f=\frac{f_s}{2}\right)\right| = L_\infty\frac{\left(\frac{f_s}{2}\right)^2}{\left(\frac{f_s}{2}\right)^2+f_r^2} = L_{f_s/2}. \quad \text{(B8)}$$

Thus,

$$10\log_{10}\left(\frac{1-2c+c^2}{1-2p+p^2}\right) - 10\log_{10}\left(\frac{1+2c+c^2}{1+2p+p^2}\right) = L_{f_s/2}. \quad \text{(B9)}$$

Similarly, as before, considering that $|p|<1$ and $|c|<1$, this expression can be simplified as

$$20\log_{10}\left(\frac{1-c}{1-p}\right) - 20\log_{10}\left(\frac{1+c}{1+p}\right) = L_{f_s/2}. \quad \text{(B10)}$$

Taking the logarithms away,

$$\frac{1-c}{1-p}\frac{1+p}{1+c} = l_{f_s/2}, \quad \text{(B11)}$$

with $l_{f_s/2} = 10^{L_{f_s/2}/20}$. Expanding and solving for p results in

$$1-c+p-cp = l_{f_s/2}(1+c-p-cp), \quad \text{(B12)}$$

$$p = \frac{(1-l_{f_s/2})+c(-1-l_{f_s/2})}{(-1-l_{f_s/2})+c(1-l_{f_s/2})}. \quad \text{(B13)}$$

Equation (B13) gives the relation that must hold between p and c for the digital system to be low pass with attenuation at $f=f_s/2$ equal to $L_{f_s/2}$ dB; and

(3) the last requirement for the digital system is that attenuation at an arbitrary frequency $f_L < f_s/2$ should also be the same as that for the continuous-time system $H(f)$ such that

$$20\log_{10}|\mathcal{H}(f=0)| - 20\log_{10}|\mathcal{H}(f=f_L)| = L, \quad \text{(B14)}$$

where

$$L = -H(f_L) = L_\infty\frac{f_L^2}{f_L^2+f_r^2}. \quad \text{(B15)}$$

Considering Eq. (B4), the previous condition results in

$$20\log_{10}\left(\frac{1-c}{1-p}\right) - 10\log_{10} \times \frac{1-2c\cos\left(2\pi\frac{f_L}{f_s}\right)+c^2}{1-2p\cos\left(2\pi\frac{f_L}{f_s}\right)+p^2} = L, \quad \text{(B16)}$$

where it has been considered again that the system is stable and minimum-phase, thus, $1\pm p$ and $1\pm c$ are always positive. Taking the logarithms away and defining $\xi = \cos(2\pi f_L/f_s)$, this third constraint results in

$$\left(\frac{1-c}{1-p}\right)^2\frac{1-2p\xi+p^2}{1-2c\xi+c^2} = 10^{L/10} = l. \quad \text{(B17)}$$

Using Eq. (B13), the denominator in the first factor can be written as

$$1-p = 1-\frac{(1-l_{f_s/2})+c(-1-l_{f_s/2})}{(-1-l_{f_s/2})+c(1-l_{f_s/2})} = -2\frac{1-c}{(-1-l_{f_s/2})+c(1-l_{f_s/2})}. \quad \text{(B18)}$$

Therefore

$$\left(\frac{1-c}{1-p}\right)^2 = \frac{1}{4}\left((-1-l_{f_s/2})+c(1-l_{f_s/2})\right)^2. \quad \text{(B19)}$$

Again considering Eq. (B13), the numerator in the second factor of Eq. (B17) can be decomposed in the following two terms

$$1+p^2 = 1+\left(\frac{\left(1-l_{f_s/2}\right)+c\left(-1-l_{f_s/2}\right)}{\left(-1-l_{f_s/2}\right)+c\left(1-l_{f_s/2}\right)}\right)^2$$
$$= \frac{2\left(1+l_{f_s/2}^2\right)+4c\left(l_{f_s/2}^2-1\right)}{\left(\left(-1-l_{f_s/2}\right)+c\left(1-l_{f_s/2}\right)\right)^2} + \frac{2c^2\left(1+l_{f_s/2}^2\right)}{\left(\left(-1-l_{f_s/2}\right)+c\left(1-l_{f_s/2}\right)\right)^2}, \tag{B20}$$

$$2p\xi = 2\xi\frac{\left(1-l_{f_s/2}\right)+c\left(-1-l_{f_s/2}\right)}{\left(-1-l_{f_s/2}\right)+c\left(1-l_{f_s/2}\right)} \times \frac{\left(-1-l_{f_s/2}\right)+c\left(1-l_{f_s/2}\right)}{\left(-1-l_{f_s/2}\right)+c\left(1-l_{f_s/2}\right)}$$
$$= 2\xi\frac{\left(l_{f_s/2}^2-1\right)+2c\left(1+l_{f_s/2}^2\right)}{\left(\left(1+l_{f_s/2}\right)+c\left(-1+l_{f_s/2}\right)\right)^2} + \frac{+c^2\left(l_{f_s/2}^2-1\right)}{\left(\left(1+l_{f_s/2}\right)+c\left(-1+l_{f_s/2}\right)\right)^2}. \tag{B21}$$

Putting the last three equations together,

$$\left(\frac{1-c}{1-p}\right)^2\left(1-2p\xi+p^2\right) = \frac{1}{2}\left(\left(1+l_{f_s/2}^2\right)+2c\left(l_{f_s/2}^2-1\right)+c^2\left(1+l_{f_s/2}^2\right) - \xi\left(l_{f_s/2}^2-1\right)+2c\xi\left(1+l_{f_s/2}^2\right)+c^2\xi\left(l_{f_s/2}^2-1\right)\right). \tag{B22}$$

Thus, Eq. (B17) can be rewritten as

$$\left(1+l_{f_s/2}^2\right)+2c\left(l_{f_s/2}^2-1\right)+c^2\left(1+l_{f_s/2}^2\right) - \xi\left(l_{f_s/2}^2-1\right)-2c\xi\left(1+l_{f_s/2}^2\right)-c^2\xi\left(l_{f_s/2}^2-1\right) = 2l\left(1-2c\xi+c^2\right), \tag{B23}$$

which is a quadratic equation with standard form

$$c^2+2c\frac{l_{f_s/2}^2-1-\xi\left(l_{f_s/2}^2-2l+1\right)}{l_{f_s/2}^2-2l+1-\xi\left(l_{f_s/2}^2-1\right)}+1=0. \tag{B24}$$

Defining $\chi = [l_{f_s/2}^2-1-\xi(l_{f_s/2}^2-2l+1)]/[l_{f_s/2}^2-2l+1-\xi(l_{f_s/2}^2-1)]$, the zero of the discrete-time system can be calculated as

$$c = \frac{-2\chi\pm\sqrt{4\chi^2-4}}{2} = -\chi\pm\sqrt{\chi^2-1}. \tag{B25}$$

The solution with $|c|<1$ should be chosen such that the system is minimum-phase.

Attenborough, K., Li, K. M., and Horoshenkov, K. (**2007**). *Predicting Outdoor Sound* (Taylor and Francis, London, UK).

Bass, H. E., Sutherland, L. C., and Zuckerwar, A. J. (**1990**). "Atmospheric absorption of sound: Update," J. Acoust. Soc. Am. **88**(4), 2019–2021.

Evans, L. B., Bass, H. E., and Sutherland, L. C. (**1972**). "Atmospheric absorption of sound: Theoretical predictions," J. Acoust. Soc. Am. **51**(5B), 1565–1575.

Gade, A. (**2007**). "Acoustics in halls for speech and music," in *Springer Handbook of Acoustics*, edited by T. D. Rossing (Springer, New York), pp. 301–350.

Hamilton, B. (**2021a**). "Adding air attenuation to simulated room impulse responses: A modal approach," in *Immersive and 3D Audio: From Architecture to Automotive*, Bologna, Italy (September 8–10, 2021) (IEEE, New York), pp. 1–10.

Hamilton, B. (**2021b**). "Air absorption filtering method based on approximate Green's function for Stokes' equation," in *International Conference on Digital Audio Effects*, Vienna, Austria (September 8–10, 2021) (IEEE, New York), pp. 160–167.

Huopaniemi, J., Savioja, L., and Karjalainen, M. (**1997**). "Modeling of reflections and air absorption in acoustical spaces—A digital filter design approach," in *Workshop on Applied Signal Processing Audio & Acoustics*, New Paltz, NY (October 19–22, 1997) (IEEE, New York), pp. 1–4.

ISO (**1993**). 9613-1:1993, "Acoustics—Attenuation of sound during propagation outdoors—Part 1: Calculation of the absorption of sound by the atmosphere" (International Standards Organizartion, Geneva, Switzerland).

Kates, J. M., and Brandewie, E. J. (**2020**). "Adding air absorption to simulated room acoustic models," J. Acoust. Soc. Am. **148**(5), EL408–EL413.

Mainolfi, P. (**2025**). "Real-time distance-extended binaural auralization in hybrid acoustic spaces," in *Immersive and 3D Audio: From Architecture to Automotive (I3DA)*, Bologna, Italy (September 10–12, 2025) (IEEE, New York), pp. 1–18.

Okuzono, T. (**2024**). "Computational accuracy and efficiency of room acoustics simulation using a frequency FEM with air absorption: 2D study," Appl. Sci. **14**(1), 194.

Oppenheim, A. V., Schafer, R. W., and Buck, J. R. (**1999**). *Discrete-Time Signal Processing*, 2nd ed. (Prentice Hall, Upper Saddle River, NJ).

Petruzzellis, C., and Zanghieri, U. (**2013**). "Digital filter for modeling air absorption in real time," in *Audio Engineering Society Convention*, Rome, Italy (May 4–7, 2013) (Audio Engineering Society, New York), Vol. 134, p. 8888.

Swiss Federal Office for Meteorology and Climatology (**2025**). "Air pressure," available at https://www.meteoswiss.admin.ch/weather/weather-and-climate-from-a-to-z/air-pressure.html (Last viewed 2025-8-2).

Tsuchiya, T. (**2007**). "Numerical simulation of sound wave propagation with sound absorption using digital Huygens' model," Jpn. J. Appl. Phys. **46**(7S), 4809–49812.